JOURNAL OF GEOPHYSICAL RESEARCH, VOL. 92, NO. C7, PAGES 6977–6986, JUNE 30, 1987

A Time-Dependent Model for Turbulent Transfer in a Stratified Oceanic Boundary Layer

MILES G. MCPHEE

McPhee Research Company, Yakima, Washington

A first-order model for vertical flux of momentum and scalars in a rotational boundary layer is applied to the oceanic boundary layer beneath sea ice. Model eddy viscosity is proportional to the product of the local friction velocity u_* and a master length scale for vertical exchange, which is a function of the rotational length scale u_*/f and the local Obukhov length L. The ratio of eddy diffusivity to eddy viscosity is 1 when turbulence is energetic but falls to lower values when turbulence levels are low and stratification high, according to an empirical relation. There are three empirical constants in the theory: ζ_N, the ratio of the master length scale to the rotational length scale; R_c, the critical flux Richardson number; and a shape factor describing the falloff of the eddy diffusivity ratio at high gradient Richardson numbers. For an idealized simulation of melting and freezing conditions representative of the marginal ice zone, the model agrees closely with a similar implementation of the Mellor-Yamada level 2.5 model. The model is demonstrated by performing a simulation of surface drift and mixed-layer properties observed during the 1984 Marginal Ice Zone Experiment field study in the Greenland Sea.

1. INTRODUCTION

The drift of sea ice is surface manifestation of currents in a turbulent oceanic boundary layer that responds primarily to surface stress, sea surface tilt, and vertical density gradients in the upper ocean. How ice drifts in response to wind reveals much about the underlying boundary layer, and simulation of ice motion is as much a problem in planetary boundary layer (PBL) physics as it is a problem in mechanics of ice deformation, especially when wind and water stress dominate the momentum equation, as they often do in the marginal ice zone. From Nansen's time [see *Ekman*, 1905] to the present, sea ice has provided a unique natural laboratory for studying rotational boundary layer turbulence.

For the most part, ice drift is modeled either by statistical techniques [*Lemke et al.*, 1980; *Thorndike and Colony*, 1982] or by direct application of the momentum balance, usually with stress between ice and water parameterized in terms of ice velocity relative to the underlying ocean. This is true even in coupled ice-ocean models [*Røed and O'Brien*, 1983; *Häkkinen*, 1986]; thus the ice/ocean drag formulation has received much attention (see, e.g., *McPhee* [1982] for a summary of several different approaches). It is sometimes useful, however, to invert the drag coefficient question by solving instead for surface velocity in terms of interfacial stress. Though this may require a more sophisticated model of the boundary layer, it has the inherent advantage of explicitly treating inertial oscillations, which are often an important part of short-term response [e.g., *McPhee*, 1980].

In a recent paper, *Mellor et al.* [1986] (hereafter referred to as MMS) applied the Mellor-Yamada "level 2.5" model to the ice/ocean boundary layer problem. Their results confirmed the importance of surface buoyancy flux in PBL dynamics (and consequently, ice drift), especially in conditions characterizing the marginal ice zone. The purpose of this paper is to introduce a time-dependent PBL model in a framework similar to MMS, but with a simplified eddy viscosity based on similarity scaling introduced by *McPhee* [1981], and to demonstrate its use in simulating drift near the ice margin. The model is used in a companion paper [*McPhee et al.*, this issue] as a template for interpreting measurements in the underice PBL during the 1984 Marginal Ice Zone Experiment (MIZEX '84).

In section 2, mathematics of the model is described, and its response compared with the Mellor-Yamada model. In section 3, it is used to simulate ice drift observed during MIZEX '84 in the Greenland Sea, demonstrating a novel method for initializing the dynamic calculations.

Paper number 7C0076.
0148-0227/87/007C-0076$05.00

2. MODEL DESCRIPTION

The time-dependent model is composed of three parts: (1) conservation equations for momentum, heat (temperature), and salt plus an approximate state equation for density variations; (2) boundary conditions, including a dynamic, free-drift ice equation and specified melt rate; and (3) techniques for initializing the solution algorithm based on kinematic analysis of drift data in the period just before the simulation. The development here parallels closely the level 2.5 model of MMS except for the following.

1. The expression for the eddy exchange coefficient in the present model is based on a heuristic combination of the planetary PBL scale, u_*/f, and the Obukhov length as described in earlier work [*McPhee*, 1981]. Though not as generally applicable as the Mellor-Yamada level 2.5 adaptation of their higher order modeling results, the present approach is simpler conceptually and numerically. Because of its simplicity, it also provides a quasi-analytic interpretation that has been used previously to model ice drift and upper ocean density structure without solving the time-dependent momentum equation [*McPhee*, 1986*a*, *b*].

2. Surface buoyancy flux is expressed in terms of measured ice ablation rates, rather than by specifying the far-field water temperature as in MMS.

2.1. *Conservation Equations*

For the turbulent boundary layer, we simplify the equations of motion and conservation of scalar quantities by assuming horizontal homogeneity, viscous processes negligible com-

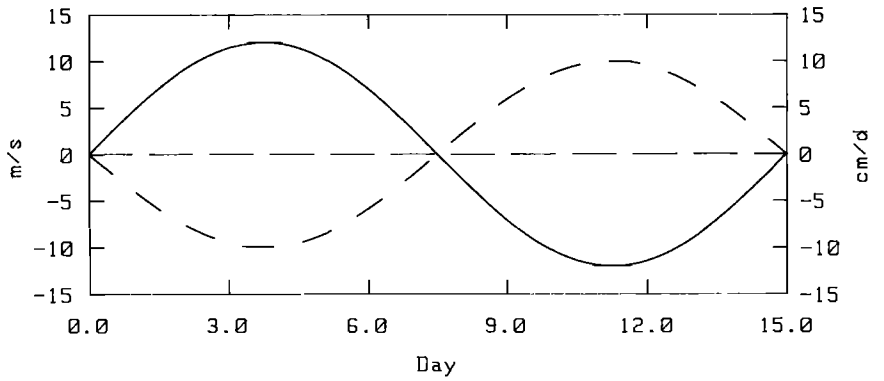

Fig. 1. Zonal (east positive) component of wind (solid line) and freezing rate (dashed line) for idealized 15-day model test. Water remains at its initial freezing temperature.

pared with turbulent transport, and turbulent motions at frequencies high relative to changes in mean boundary layer properties (i.e., a "spectral gap" exists). Under these conditions the advective terms in the momentum equation reduce to the vertical gradient of the covariance between vertical and horizontal fluctuating velocities, which may be identified as "turbulent stress:"

$$\frac{\partial \hat{u}}{\partial t} + if\hat{u} = \frac{\partial \hat{\tau}}{\partial z} = \frac{\partial}{\partial z}\left(K\frac{\partial \hat{u}}{\partial z}\right)$$

$$\hat{\tau} = -(\langle u'w'\rangle + i\langle u'v'\rangle)$$

where for convenience, the horizontal velocity vector is expressed as a complex number $\hat{u} = u + iv$ (where $i^2 = -1$). Conservation equations for scalar temperature and salinity are similarly written:

$$\frac{\partial \theta}{\partial t} = -\frac{\partial \langle w'\theta'\rangle}{\partial z} = \frac{\partial}{\partial z}\left(\alpha_\theta K\frac{\partial \theta}{\partial z}\right)$$

$$\frac{\partial S}{\partial t} = -\frac{\partial \langle w'S'\rangle}{\partial z} = \frac{\partial}{\partial z}\left(\alpha_S K\frac{\partial S}{\partial z}\right)$$

K is the eddy viscosity, α_θ is the ratio of kinematic eddy viscosity to turbulent heat diffusivity (turbulent Prandtl number), and α_S is the ratio of eddy viscosity to turbulent salt diffusivity (turbulent Schmidt number).

2.2. *First-Order Closure*

The expression for eddy viscosity follows from similarity conditions described in an earlier work [*McPhee*, 1981], where we showed that beyond a thin surface layer, profiles of velocity, stress, and eddy viscosity are similar in boundary layers stabilized by surface buoyancy flux, if nondimensionalized by the following scales: vertical displacement $u_*\eta_*/f$, turbulent stress u_*^2, mean current speed u_*/η_*, and eddy viscosity $u_*^2\eta_*^2/f$, where η_* is a stability parameter that characterizes the effect of buoyancy on boundary layer extent and velocity:

$$\eta_* = \left(1 + \frac{\xi_N u_*}{fR_cL}\right)^{-1/2}$$

where ξ_N is a dimensionless constant, R_c is the critical flux Richardson number, equal to 0.2, and L is the Obukhov length,

$$L = \frac{\rho_0 u_*^3}{gk\langle\rho'w'\rangle}$$

where ρ_0 is reference density, g is the acceleration of gravity, k is von Karman's constant (0.4), $\langle\rho'w'\rangle$ is turbulent mass flux, and u_* is friction velocity:

$$u_* = \tau^{1/2} = |\langle u'w'\rangle + i\langle v'w'\rangle|^{1/2}$$

Generalizing from the earlier work, the length scale describing the vertical scale of "energy-containing" eddies at any level in the flow is given by

$$\lambda = \xi_N u_* \eta_*^2/f = \frac{\xi_N u_*}{f[1 + (\xi_N u_*)/(R_c fL)]} \quad (1)$$

For small Obukhov length (strong buoyancy), λ is approximately R_cL. If stratification is neutral, $\eta_* = 1$ and $\lambda = \xi_N u_*/f$. By considering pack ice drift in summer, we estimated ξ_N to be about 0.05 [*McPhee*, 1981]. In the neutrally stratified region (well-mixed layer) of a typical underice boundary layer, λ is 3–4 m.

When buoyancy flux is negative (unstable), the length scale is allowed to grow following (1), except that it is limited to $10\xi_N u_*/f$, which is 10 times the neutral maximum. The length scale in this formulation represents the vertical influence of dominant eddies in the flow and is more responsive to buoyancy than the master length scale in the Mellor-Yamada model, which is related to the correlation scale of the eddies. In the latter model, buoyancy enters the K calculations through the shape factors S_m and S_h [*Mellor and Yamada*, 1982].

Eddy viscosity is

$$K = ku_*\lambda \qquad |z| \geq \lambda$$

$$K = ku_*z \qquad |z| < \lambda$$

Mass flux is estimated from temperature and salinity flux:

$$\frac{\langle\rho'w'\rangle}{\rho_0} = -\beta_\theta\langle w'\theta'\rangle + \beta_S\langle w'S'\rangle$$

$$= \beta_\theta\alpha_\theta K\frac{\partial \theta}{\partial z} - \beta_S\alpha_S K\frac{\partial S}{\partial z}$$

where β_θ and β_S are expansion coefficients for temperature and salinity, taken from *Gill* [1982, table A3.1].

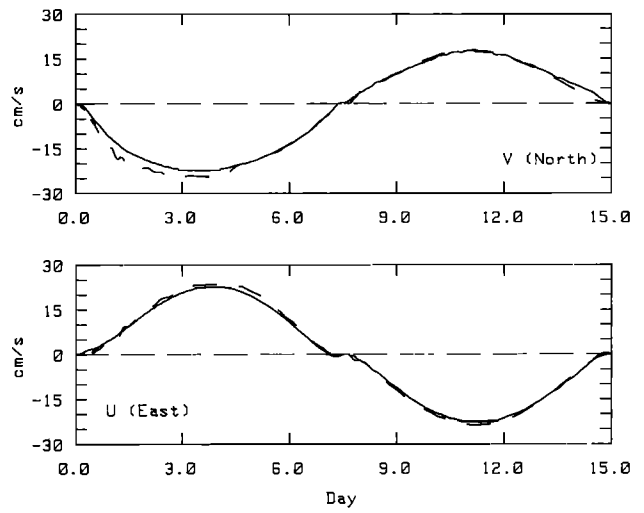

Fig. 2. Comparison of surface velocity for idealized simulation as calculated by the present model (solid line), with the Mellor-Yamada level 2.5 model of MMS (dashed line). Underice surface roughness is 0.05 m for each model.

Turbulent diffusivities for heat and salt are related to eddy diffusivity by the factors α_θ and α_S. In a fully turbulent regime like that found in the mixed layer near the ice-ocean interface, inertial terms in the conservation equations completely dominate viscous terms (i.e., the Reynolds number is high), and by Reynold's analogy, the ratio of scalar diffusivity to eddy viscosity approaches unity. Deeper in the mixed layer, turbulence levels fall, and in the highly stratified fluid near the top of the pycnocline, the turbulence becomes intermittent as mean flow shear interacts with internal waves. *Turner* [1973, chap. 5] points out that under these conditions, pressure forces in the momentum equation, which have no analog in the θ and S conservation equations, can transfer momentum more readily than heat or salt are transported by direct turbulent overturn, so that the effective average eddy viscosity may be much larger than the eddy diffusivities for heat and salt, though all are larger than molecular values (because "patchy" turbulence still accounts for most of the vertical exchange). Thus we impose on α_θ and α_S the condition that they be close to 1 in the fully turbulent regime characterizing most of the mixed layer, but fall off as turbulence decreases and mean stratification increases. This suggests a gradient Richardson number dependence, and we use an implicit form of the equation suggested by *Turner*'s [1973] equation 5.2.23, from work by *Ellison* [1957], viz.,

$$\alpha_S = \alpha_\theta = \alpha = \frac{b[1 - (\alpha Ri/R_c)]}{(1 - \alpha Ri)^2}$$

where

$$Ri = \frac{(-g/\rho_0)(\partial\rho/\partial z)}{|\partial\hat{u}/\partial z|^2} = \frac{gK^2}{\tau^2}\left(\beta_\theta \frac{\partial\theta}{\partial z} - \beta_S \frac{\partial S}{\partial z}\right)$$

For $Ri < 0.05$, $\alpha = 1$, and for $Ri \geq 5$, $\alpha = \alpha(5)$, which is about 0.03 for $b = 1.4$ and $R_c = 0.2$.

2.3. *Boundary Conditions*

In the implicit numerical solution [see, e.g., *Lapidus and Pinder*, 1982], eddy diffusivities are calculated based on turbulent stress and density structure from the previous time step, with a free-drift, dynamic boundary condition at the ice-ocean interface:

$$\frac{\partial\hat{u}_0}{\partial t} + if\rho_i h\hat{u}_0/\rho_0 = \hat{\tau}_a - K\left.\frac{\partial\hat{u}}{\partial z}\right|_0$$

where $\rho_i h$ is the mass per unit area of the ice cover and $\hat{\tau}_a$ is the applied wind stress, divided by reference water density. At the lower boundary, stress vanishes, and velocity matches an imposed geostrophic velocity, taken to be zero in the examples here. A general method for prescribing initial conditions is presented in the next section; in the following example, the ice-ocean system is started from rest.

2.4. *Idealized Demonstration*

An idealized forcing that combines variable wind stress with variable surface buoyancy flux is used to test the model

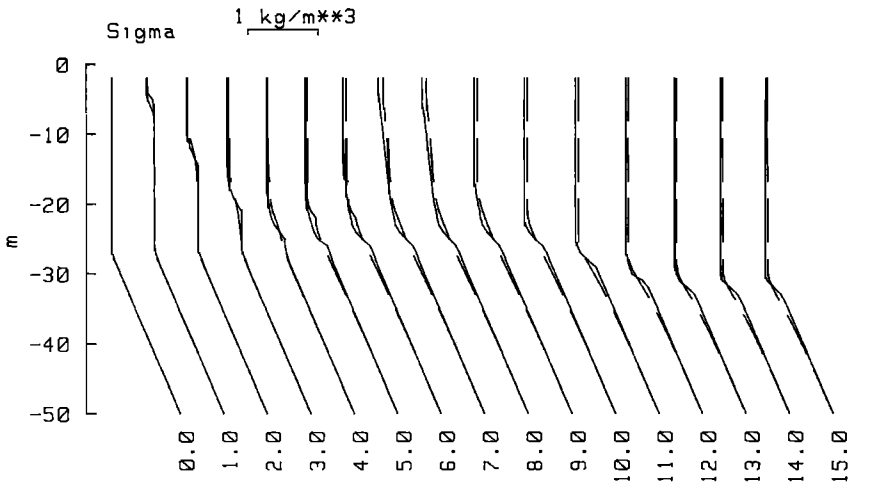

Fig. 3. Density profiles on successive days of the model calculations. Numbers at base of profiles indicate time in days from startup. Present model, solid line; Mellor-Yamada, dashed line.

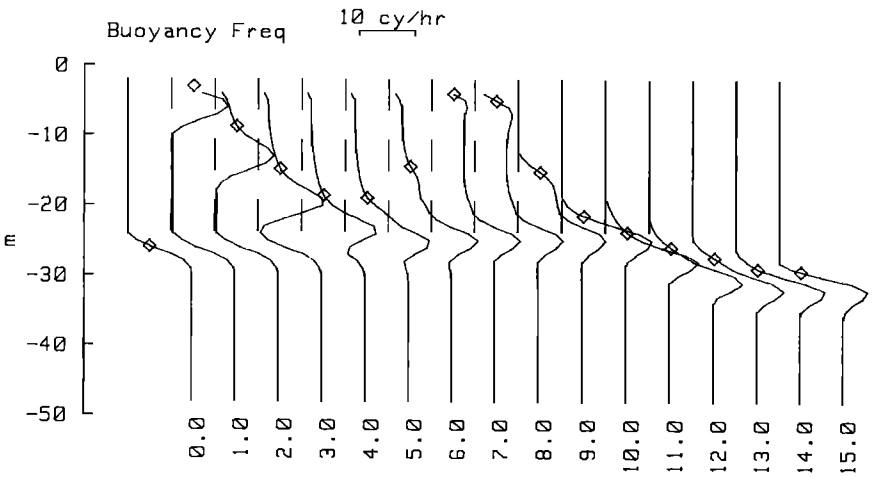

Fig. 4. Buoyancy frequency profiles corresponding to the model density profiles of Figure 3. Diamonds mark the level at which the buoyancy frequency exceeds 4 cph, taken to be the mixed-layer depth.

against the Mellor-Yamada level 2.5 model of MMS. Over a 15-day cycle, the zonal wind magnitude and ice melt rate vary sinusoidally with time as shown in Figure 1, with zero net wind and ice growth. The Coriolis parameter is 1.45×10^{-4} s^{-1} (90° N), and the underice roughness length is 5 cm. The air drag coefficient is 2.3×10^{-3}. Initial ice thickness is 2 m. Water temperature is set to its initial freezing temperature and remains there (i.e., there is no heat flux at the ice-ocean interface). We assume that none of the heat required to melt ice comes from the ocean but is instead furnished by thermodynamic processes within the ice-atmosphere system. This is not entirely realistic; some heat flux must occur to prevent supercooling as the water column freshens, and even in the high Arctic, the ocean absorbs enough solar radiation in summer to heat the mixed layer by 0.1–0.2°C above freezing. Nevertheless, buoyancy flux at low temperatures is controlled almost entirely by salinity because the thermal expansion coefficient is small; thus neglecting heat flux has very little impact on the dynamics. Salinity flux is proportional to melt rate, and the test case is chosen so that the highest wind stress occurs with maximum melting (maximum positive surface buoyancy) in the first half cycle and with maximum freezing in the second half. The wind changes slowly enough that inertial oscillations are minimal, as shown in the surface ice velocity of both models (Figure 2). Evolution of the density structure from the initial 25-m mixed layer (Figure 3) shows formation of a shallow fresh layer as the ice begins to melt, which is mixed downward as wind increases. Maximum mixing is limited, however, by the stabilizing influx of melt water. As the wind slacks on days 7 and 8, the upper ocean is stratified almost to the surface. In the second half cycle, buoyancy flux is unstable, and rapid deepening of the mixed layer occurs as wind stress picks up again. The layer continues to deepen slowly as wind slacks in the last quarter because the surface buoyancy is still negative.

There is little difference between the models in their simulation of upper ocean density structure, except for a tendency of the Mellor model to smear the sharp density gradients (Figure 3). In order to define a "mixed layer," even when there is stabilizing buoyancy at the surface, we consider buoyancy (Brunt-Väisälä) frequency profiles, calculated from density gradients, shown in Figure 4, and define the mixed-layer depth as the uppermost depth at which the buoyancy frequency exceeds 4 cph ($N = 0.007$ s^{-1}). With this definition, mixed-layer depth and salinity over the 15-day cycle are compared in Figure 5.

Both models explicitly calculate velocity and turbulent stress at each level in the computational domain. Hodographs of velocity and stress, averaged over the stable and unstable halves of the cycle, are compared at selected levels in Figure 6. Again, agreement is quite close. Rightward turning of the velocity and horizontal traction vectors with depth results from the Coriolis acceleration and is well documented in the boundary layer under sea ice [e.g., *McPhee et al.*, this issue]. Note that velocities near the surface in the unstable cycle (day 7.5–15) are smaller than in the first half, indicating increased

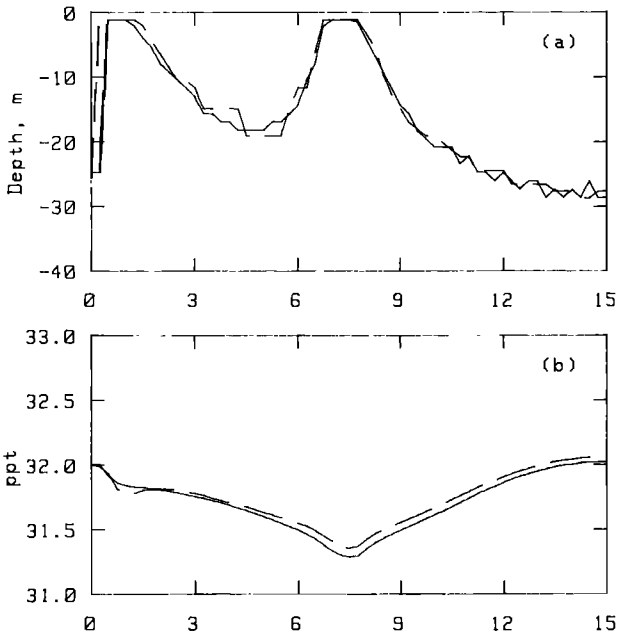

Fig. 5. (*a*) Mixed-layer depth as a function of time: present model (solid line) and Mellor-Yamada (dashed line). (*b*) As in Figure 5*a* except mixed-layer salinity.

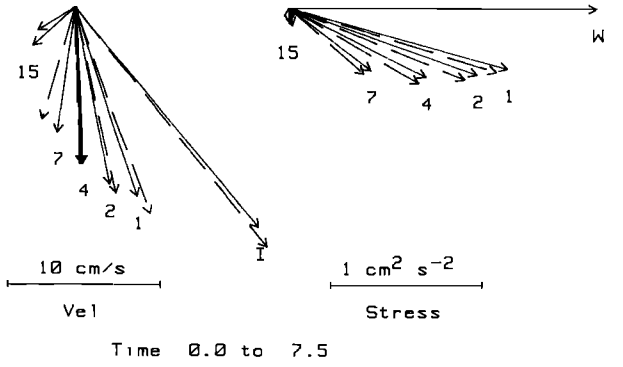

Fig. 6a

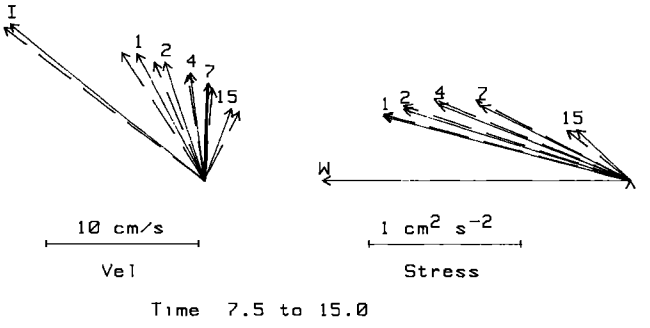

Fig. 6b

Fig. 6. Plan view of mean velocity and horizontal turbulent stress at selected levels. Numbers at vector tips indicate depth below the ice undersurface; Point I indicates ice velocity; point W indicates wind stress. Up is north. Solid vectors are from present model; dashed from Mellor-Yamada model. (*a*) Averaged over the first half of the simulation, with ice melting (stable buoyancy) and westerly wind. (*b*) Averaged over second half of simulation, with freezing (unstable buoyancy) and easterly wind.

drag: buoyancy effects cause hysteresis in the ice drift relative to the progressive wind vector, which shows up to about the same degree in each model.

3. MIZEX Simulations

In this section the model is demonstrated by simulating upper ocean response and ice drift near the research vessel *Polar Queen*, which was moored to a large floe and allowed to drift passively during MIZEX '84. We consider a 12-day period from day 172 to day 184 because the ship remained over a reasonably uniform water mass, despite highly variable wind and drift conditions. The upper ocean was not horizontally homogeneous during this entire period; however, horizontal gradients in average heat and salinity of the upper water column were minor compared with most other periods during the drift. Thus there is some hope that a one-dimensional model can capture the essential physics. We proceed as follows. First, kinematic analysis of ship navigation data is used to estimate "mean," inertial, and tidal components of ice drift. Wind stress is taken from surface wind measured at the floe using the drag coefficient ($c_{10} = 2.3 \times 10^{-3}$) determined by profile and direct stress measurements (P. Guest, personal communication, 1986). Short gaps in the wind record were filled by linear interpolation, and the entire record

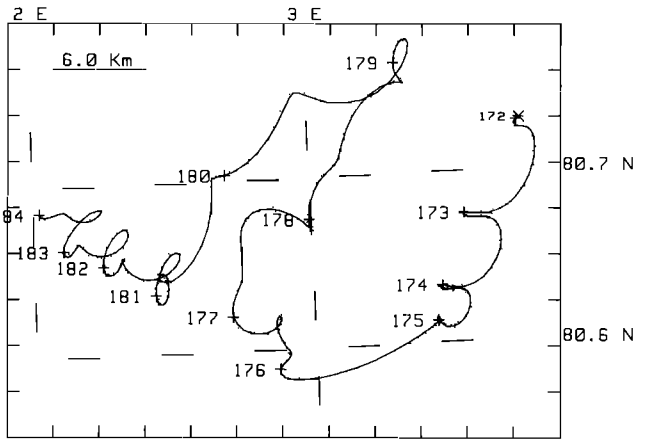

Fig. 7. Fitted trajectory of the *Polar Queen* as she drifted passively with the ice, days 172–184 (solid line). Dots indicate each raw position fix from the satellite navigator used in the complex demodulation.

was filtered with a 3-hour running mean. We estimate surface buoyancy flux from the average bottom and surface ablation measured daily [*Maykut and Perovich*, 1985]. Salinity and temperature profiles from the Arctic profiling system (APS) (J. Morison, personal communication, 1986) are used to set the initial temperature and salinity profiles. We show how the inertial component derived from drift prior to the simulation period may be combined with a steady state variant of the numerical model to initialize the time-dependent calculation under almost any conditions, eliminating the need for "ramping" the model or filtering spurious inertial oscillations. The technique is demonstrated by a short simulation. We then calculate surface drift and mixed-layer characteristics for the entire 12-day period.

Kinematic analysis is accomplished with a "complex demodulation" technique [*McPhee*, 1986*a*], which is recapped briefly here. We assume that an ice drift trajectory consists of a superposition of mean motion, plus circular or elliptical oscillations at the inertial (or semidiurnal) and diurnal tidal frequencies. In most of the Arctic, the diurnal tidal signal is small; however, *Hunkins* [1986] found a strong diurnal component in current meter records from over the Yermak Plateau just northeast of the region through which the *Polar Queen* drifted, and we show below that it is an important element in the *Polar Queen* drift. We thus write the instantaneous velocity as a complex vector:

$$\hat{V}(t) = \hat{V}_m + \hat{S}_{cw}e^{-ift} + \hat{S}_{ccw}e^{ift} + \hat{D}_{cw}e^{-i\omega t} + \hat{D}_{ccw}e^{i\omega t} \qquad (2)$$

where f is the angular frequency of the inertial (or semidiurnal tidal) oscillations with amplitude and phase of clockwise and counterclockwise components described by $\hat{S}_{cw}$ and $\hat{S}_{ccw}$, respectively. The diurnal tidal ellipse is similarly described by ω, $\hat{D}_{cw}$, and $\hat{D}_{ccw}$, where ω is the angular frequency of diurnal tide. The circumflex denotes complex numbers; vector quantities written without a circumflex denote magnitude.

The data for determining velocity are satellite navigation fixes, randomly spaced in time, usually with 35–40 good fixes available per day. To relate these to (2), the velocity is integrated from initial position $\hat{X}_0$:

$$\hat{X} = \hat{X}_0 + \hat{V}_m t + (i/f)[\hat{S}_{cw}(e^{-ift} - 1) + \hat{S}_{ccw}(1 - e^{ift})] + (i/\omega)[\hat{D}_{cw}(e^{-i\omega t} - 1) + \hat{D}_{ccw}(1 - e^{i\omega t})] \qquad (3)$$

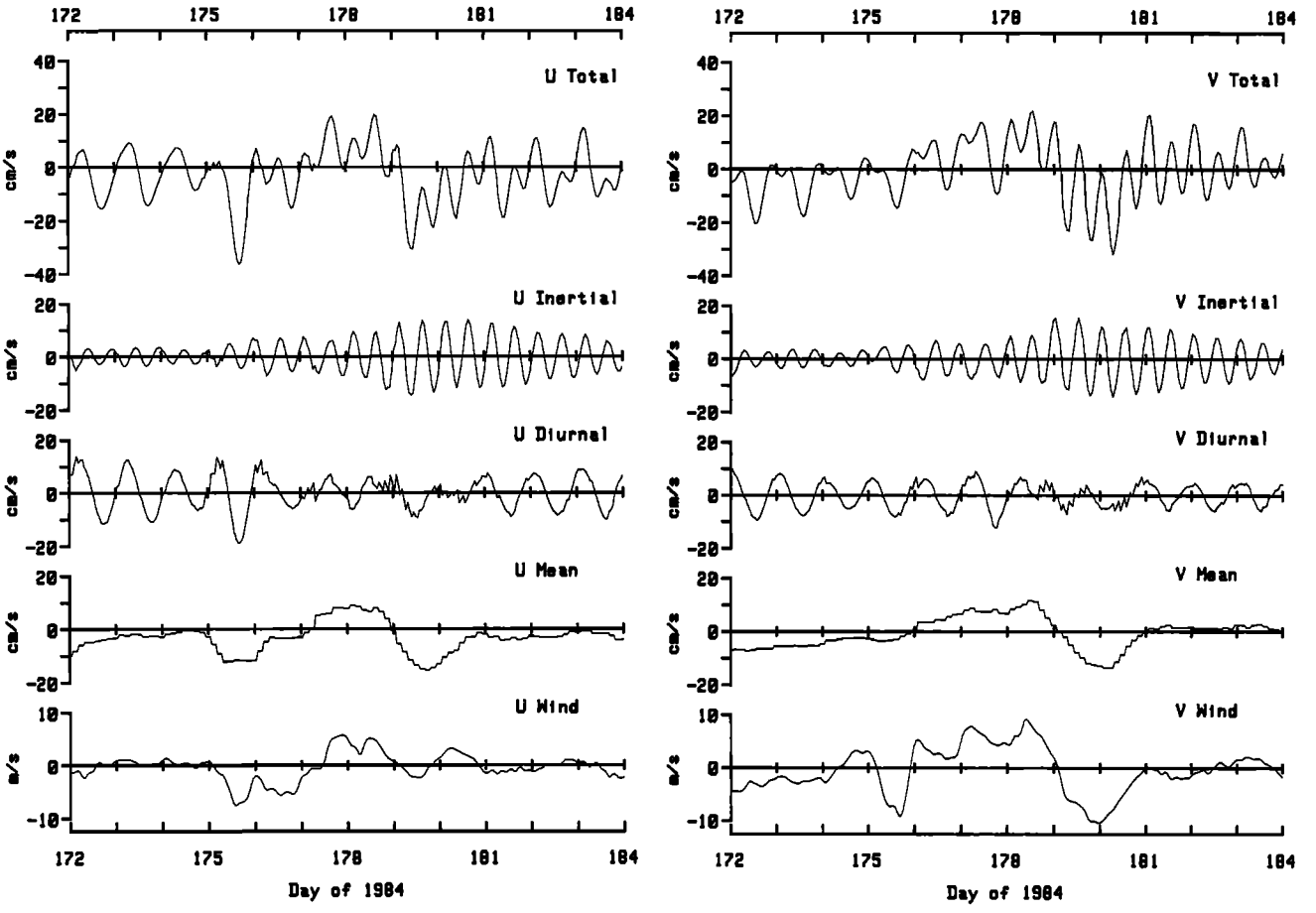

Fig. 8a

Fig. 8b

Fig. 8. Separated components of ice velocity, showing total, inertial, diurnal tidal, and mean decompositions, along with observed 10-m wind. (*a*) Eastward positive, west negative. (*b*) Northward positive, south negative.

By considering all fixes in a period comparable to the period of the longest oscillation, we may write a system of linear equations for the six complex coefficients that minimizes mean-square errors between the position data and the function (3). The resulting matrix equation is solved by Gaussian elimination. Time evolution of the mean velocity vector and the oscillatory coefficients (phasors) is calculated by advancing the fit window through the data at time steps smaller than the width of the window.

The drift trajectory fitted every 3 hours from data in the preceding and succeeding 12 hours, for the period from day 172 to day 184, is shown in Figure 7, along with each raw fix used in the fitting scheme. Corresponding velocity components are shown in Figure 8, along with the wind, plotted on a "2% scale." Note the prevalence of both inertial and diurnal oscillations, especially in the complicated looping after day 180. We expect inertial oscillations because of the prominent role played by the Coriolis force in the equations of motion; however, there is no analogous effect at the diurnal frequency, and we assume that the diurnal oscillations result from processes outside the wind/ice/boundary layer system [e.g., *Hunkins*, 1986]. Wind and mean drift are obviously correlated, with drift generally clockwise from the wind vector.

On days 179–180, there is rapid drift to the southwest in northerly winds, with energetic inertial oscillation. The combination of existing inertial motion, coupled with a strong mean velocity, provides a good test of the initialization procedure. Figure 9 illustrates why correctly specifying the initial momentum of the ice/mixed-layer system is necessary for simulating motion in the first few inertial periods. The model is started from rest with the observed temperature, salinity, and wind at time 180.0. The impulsive forcing introduces a spurious inertial oscillation, which as it turns out, is almost completely out of phase with the actual inertial motion. To properly specify the initial condition requires estimating the total momentum of the boundary layer due to turbulent shear stress, which we accomplish by (1) calculating the mean velocity in the PBL, which would be in steady state equilibrium with the initial wind, and (2) adding the inertial velocity determined from the drift track prior to the initialization time.

The equilibrium velocity is obtained by solving the steady PBL equation

$$if\hat{u} = \frac{\partial}{\partial z}\left(K\frac{\partial \hat{u}}{\partial z}\right)$$

subject to the boundary condition

$$if\rho_i h\hat{u}_0/\rho_0 = \hat{\tau}_a - K\frac{\partial \hat{u}}{\partial z}\bigg|_0$$

Since K depends on the stress state in the water column, which is unknown initially, the solution is obtained by iter-

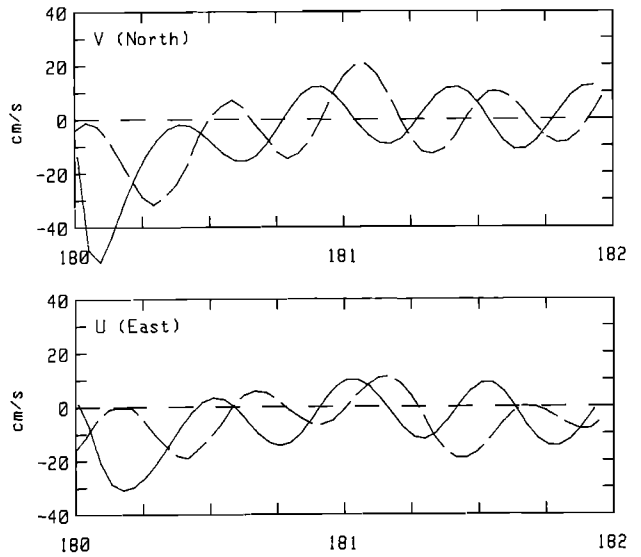

Fig. 9. Two-day simulation of surface velocity, with model started from rest (solid line), compared with observed velocity (dashed line). Note the phase shift in inertial oscillations.

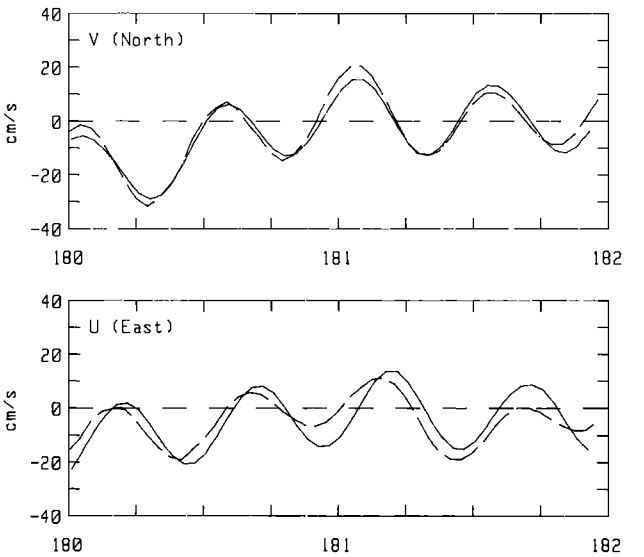

Fig. 11. Two-day simulation as in Figure 9, except with initial velocity set to steady state solution plus fitted inertial component in the mixed layer.

ation, starting with

$$K = ku_{*a}z \qquad |z| \le \xi_N u_{*a}/f$$

$$K = k\xi_N u_{*a}{}^2\xi/f \qquad |z| > \xi_N u_{*a}/f$$

$$u_{*a} = (\rho_a c_{10}/\rho_0)^{1/2} U_{10}$$

Given a first estimate of K, velocity and stress are calculated implicitly from the upper boundary condition, then K is recalculated, taking into account the density structure. The process is repeated (Figure 10) until the integrated change in K from one iteration to the next falls below some tolerance.

After the equilibrium velocity profile is calculated, the inertial velocity $\hat{V}_{in}$ is added to velocities in the mixed layer, where the mixed layer extends to the depth at which K has decreased to 10% of its maximum value. The inertial component is given by

$$\hat{V}_{in} = \hat{S}_{cw} e^{-if(t_s - t_0)}$$

where t_s is the time at startup, t_0 is the reference time for the complex demodulation, and $\hat{S}_{cw}$ is the clockwise, semidiurnal phasor, evaluated at $t_s - 12$ hours.

The same simulation as Figure 9, except with the initial velocity structure prescribed by the procedure described above, is shown in Figure 11. The slight phase shift in the inertial oscillation at the beginning of the simulation occurs because the startup inertial velocity is calculated from the $\hat{S}_{cw}$ phasor evaluated for the time centered 12 hours before 180.0. The shift indicates that the phasor has rotated slightly in the intervening time. Note that wind data are the only measurements used after time 180.0.

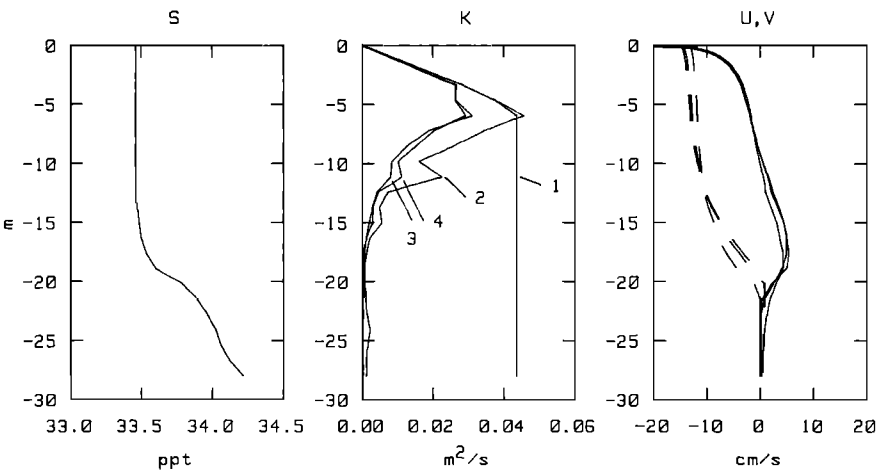

Fig. 10. Successive iterations of the steady state model used for initialization. The first eddy viscosity profile, line 1, increases linearly to a constant value for the outer layer, which is used to calculate velocity profiles (u, solid line; v, dashed line). Stress is then calculated, and the eddy viscosity estimate refined according to the density structure (indicated by the observed salinity profile). The process is repeated (as indicated by K profiles 2–4) until a convergence criterion is satisfied.

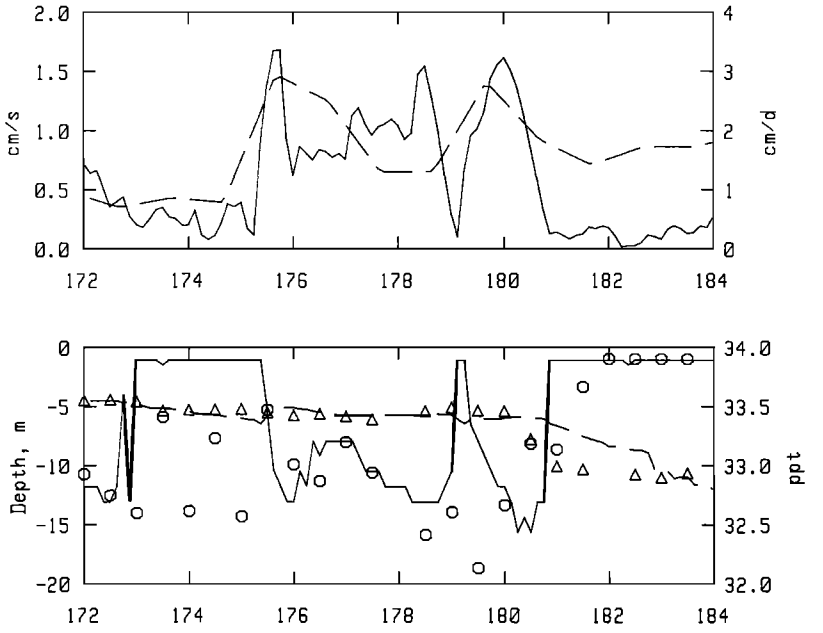

Fig. 12. (Top) Model interface friction velocity u_* (solid line) and prescribed melt rate (dashed line), adapted from *Maykut and Perovich* [1985]. (Bottom) Model mixed-layer depth (solid line) and modeled mixed-layer salinity (dashed line). Circles are mixed-layer depths every 12 hours, from APS measurements (J. Morison, personal communication, 1986); triangles are measured mixed-layer salinity. Mixed-layer depth is defined as the level (past 1 m) where the Brunt-Vaisala frequency exceeds 4 cph in both model and data. If stratification persists to the surface, the mixed-layer depth is shown as being 1 m from the ice undersurface.

A complete simulation for the period from day 172 to day 184 was calculated using the observed wind and initial conditions at time 172.0. We assumed for this run that heat added to the water column was immediately extracted as ice melt. This was not rigorously true, as the mixed layer sometimes rose a few tenths of a degree above its freezing point. However, the effect on buoyancy is minor (because the thermal expansion coefficient is small at low temperature); thus we treated the meltwater as a salinity flux, based on the combined surface and bottom ablation. We reasoned that any storage of water on the surface (in melt ponds and slush) was compensated by melting at floe edges. During this 12-day period, ice concentration around the *Polar Queen* appeared to be 9/10 or higher, and the average ablation was of the order of 2 cm d^{-1}. Melt rate and interfacial friction velocity are weakly correlated (Figure 12), as we might expect, since bottom ablation, which occurs by turbulent heat transfer from the ocean, increases with increasing turbulence.

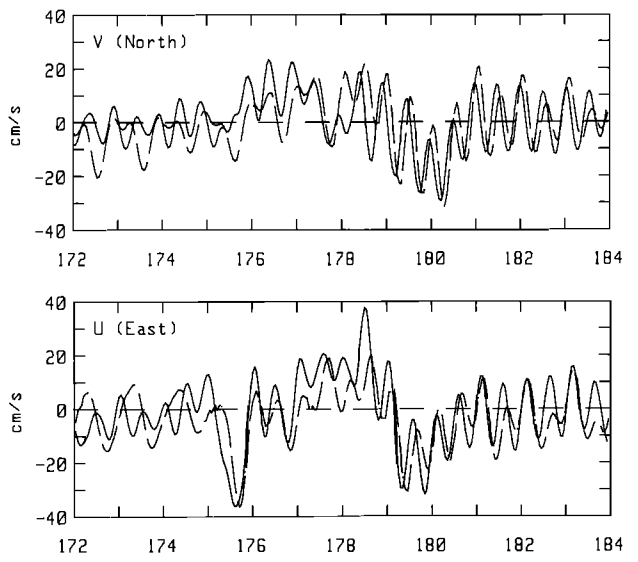

Fig. 13. Twelve-day simulation of surface velocity (solid line) compared with observed velocity (dashed line).

Mixed-layer depth and salinity are shown in Figure 12. As before, mixed-layer depth is defined by the level at which the buoyancy frequency exceeds 4 cph. Although this definition is somewhat arbitrary, it better allows comparison with data than one based, say, on eddy viscosity. Except for the period of low stress and melt rate from days 173 to day 175, the model agrees reasonably well with APS samples measured every 12 hours. Overall, the initial stratification and continuous positive surface buoyancy flux tend to keep the mixed layer very shallow, even when interfacial stress exceeds 0.2 Pa.

Surface drift velocity is shown in Figure 13, along with the fitted observations. In general, the major features of the 12-day drift are reproduced quite well, considering the complexity of the system and the simplicity of the model (we have neglected, for example, geostrophic currents associated with dynamic topography across Fram Strait). Some of the short-term difference between the model and observations is reduced by adding the 24-hour tide to the model output (Figure 14).

4. CONCLUSION

We have introduced a numerical model for turbulence in rotational boundary layers based on a relatively simple expression for the scale of energy-containing eddies and the cor-

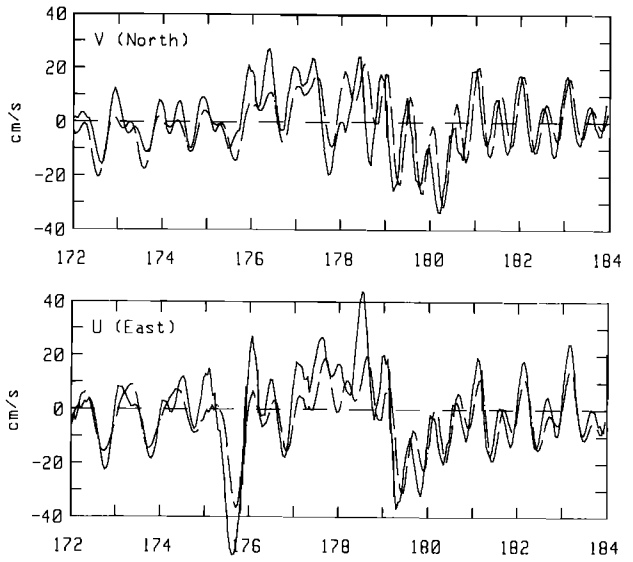

Fig. 14. Same as Figure 13, except diurnal tidal component added to modeled velocity.

responding eddy diffusivity. The basic premise of the scaling [*McPhee*, 1981] is that in the free turbulence of the PBL beyond a thin surface layer adjacent to either the air-sea interface or a solid boundary, the length scale depends on the rotational scale, $\xi_N u_*/f$, and the local Obukhov length, L, such that whichever scale is smaller tends to dominate. Eddy diffusivities for scalar quantities such as salt and heat are the same as for momentum, except when turbulence levels are low and stratification high, in which case the ratio of the diffusivities follows a gradient Richardson number dependence suggested by *Turner* [1973]. There are relatively few adjustable constants in the theory. They are the critical flux Richardson number R_c, taken to be 0.2, a constant characterizing the nondimensional maximum eddy length in neutral conditions ξ_N, taken to be about 0.05 based on observed drift of sea ice, and b (= 1.4 [after *Turner*, 1973]), a shape factor that determines how fast the ratio of scalar eddy diffusivity to eddy viscosity falls off at high-gradient Richardson numbers. The theory is relatively insensitive to the last parameter.

In numerical simulations of an idealized regime with a 15-day cycle in surface stress and surface buoyancy, and a preexisting density gradient at depth, the present model is shown to be in close agreement with the Mellor-Yamada level 2.5 model derived from second-order closure of the equations of motion. The Mellor model is becoming a standard by which oceanic and atmospheric PBL models are judged because it applies knowledge gained by decades of careful laboratory and field turbulence experiments to a comprehensive term-by-term analysis of the second-moment equations and produces a framework that, without modification, explains many seemingly disparate flow regimes [*Mellor and Yamada*, 1982].

The basis of the present model is different, albeit less ambitious. It derives from the similarity concepts described by *McPhee* [1981], in which we took some well-known gross characteristics of planetary boundary layers, including Rossby-similarity scaling [see, e.g., *McPhee*, 1979] and reduction of drag with increasing stability [e.g., *Clarke and Hess*, 1974] and fitted them into the fundamental mixing length hypothesis of turbulent exchange based in part on surface layer ideas advanced by *Businger and Arya* [1974] and *Zilitinkevich* [1975]. From this we identified a vertical scale for the largest, energy-containing eddies in the PBL and the limiting depth to which free turbulence penetrates. When placed in the context of a time-dependent numerical model of the oceanic boundary layer with a realistic pycnocline, the close correspondence of the present model with the Mellor model, despite their different derivations, suggests that the scaling arguments have merit. The advantage of the present technique is its conceptual and numerical simplicity.

NOTATION

b shape factor in eddy diffusivity ratio.
c_{10} ten-meter wind drag coefficient.
$\hat{D}_{cw}$, $\hat{D}_{ccw}$ phasors describing the clockwise and counterclockwise rotary motion at the diurnal tidal frequency.
f Coriolis angular frequency.
g acceleration of gravity, equal to 9.8 m s^{-2}.
h ice thickness.
i imaginary number.
k von Karman's constant.
K eddy viscosity.
L Obukhov length, equal to $\rho_0 u_*^3/(gk\langle\rho' w'\rangle)$.
S salinity.
$\hat{S}_{cw}$, $\hat{S}_{ccw}$ phasors describing the clockwise and counterclockwise rotary motion at the inertial (semidiurnal) frequency.
$\hat{u}$ complex water velocity.
$\hat{u}_0$ complex surface (ice) velocity.
u_* friction velocity, local, equal to $\tau^{1/2}$.
u_{*a} friction velocity based on air stress.
$\hat{U}_{10}$ complex surface wind.
$\langle w'\theta'\rangle$, $\langle w'S'\rangle$, $\langle\rho' w'\rangle$ turbulent temperature, salinity, and density flux.
$\hat{V}$ total complex velocity in complex demodulation scheme.
$\hat{V}_{in}$ complex mixed-layer inertial velocity.
$\hat{V}_m$ complex mean velocity, $\hat{V}$ minus inertial and tidal velocities.
α, α_θ, α_S ratios of eddy diffusivity to eddy viscosity.
β_θ, β_S thermal expansion coefficients for temperature and salinity.
θ water temperature.
λ master vertical eddy length scale.
ξ_N nondimensional mixing length in the neutral PBL.
ρ_0, ρ_i, ρ_a reference densities for water, ice, and air.
$\hat{\tau}$ complex turbulent stress in the water column.
$\hat{\tau}_a$ complex wind stress, equal to $(\rho_a/\rho_0)c_{10}U_{10}\hat{U}_{10}$.

Acknowledgments. I am indebted to G. Mellor of Princeton University for furnishing the Mellor-Yamada level 2.5 model and for his thoughtful advice and guidance. I also thank P. Guest and K. Davidson of the Naval Postgraduate School, and G. Maykut and J. Morison of the University of Washington for furnishing data. This work was supported financially by the Office of Naval Research contract N-00014-84-C-0028.

References

Businger, J. A., and S. P. S. Arya, The height of the mixed layer in a stably stratified planetary boundary layer, *Adv. Geophys., 18A*, 73–92, 1974.

Clarke, R. H., and G. D. Hess, Geostrophic departure and the functions A and B of Rossby-number similarity theory, *Boundary Layer Meteorol., 7*, 267–287, 1974.

Ekman, V. W., On the influence of the earth's rotation on ocean currents, *Ark. Mat. Astron. Fys., 2*, 1–52, 1905.

Ellison, T. H., Turbulent transport of heat and momentum from an infinite rough plane, *J. Fluid Mech., 2*, 456–466, 1957.

Gill, A. E., *Atmospheric-Ocean Dynamics*, 661 pp., Academic, Orlando, Fla., 1982.

Häkkinen, S., Coupled ice-ocean dynamics in the marginal ice zones: Upwelling/downwelling and eddy generation, *J. Geophys. Res., 91*, 819–832, 1986.

Hunkins, K., Anomalous diurnal tidal currents on the Yermak Plateau, *J. Mar. Res., 44*, 51–69, 1986.

Lapidus, L., and G. F. Pinder, *Numerical Solution of Partial Differential Equations in Science and Engineering*, 677 pp., John Wiley, New York, 1982.

Lemke, P., E. W. Trinkl, and K. Hasselmann, Stochastic dynamic analysis of polar sea ice variability, *J. Phys. Oceanogr., 10*, 2100–2120, 1980.

Maykut, G. A., and D. K. Perovich, MIZEX 84 heat and mass balance data, *Tech. Rep. APL-UW 12-85*, 73 pp., Univ. of Washington, Seattle, 1985.

McPhee, M. G., The effect of the oceanic boundary layer on the mean drift of pack ice: Application of a simple model, *J. Phys. Oceanogr., 9*, 388–400, 1979.

McPhee, M. G., A study of oceanic boundary-layer characteristics including inertial oscillation at three drifting stations in the Arctic Ocean, *J. Phys. Oceanogr., 10*, 870–884, 1980.

McPhee, M. G., An analytic similarity theory for the planetary boundary layer stabilized by surface buoyancy, *Boundary Layer Meteorol., 21*, 325–340, 1981.

McPhee, M. G., Sea ice drag laws and simple boundary layer concepts, including application to rapid melting, *CRREL Rep. 82-4*, U.S. Army Cold Regions Res. and Eng. Lab., Hanover, N. H., 1982.

McPhee, M. G., Analysis and prediction of short-term ice drift, paper presented at the Fifth International Offshore Mechanics and Arctic Engineering Symposium, Am. Soc. of Mech. Eng., Tokyo, April 13–18, 1986*a*.

McPhee, M. G., The upper ocean, in *The Geophysics of Sea Ice*, edited by N. Untersteiner, pp. 339–394, Plenum, New York, 1986*b*.

McPhee, M. G., G. A. Maykut, and J. H. Morison, Dynamics and thermodynamics of the ice/upper ocean system in the marginal ice zone of the Greenland Sea, *J. Geophys. Res.*, this issue.

Mellor, G. L., and T. Yamada, Development of a turbulence closure model for geophysical fluid problems, *Rev. Geophys., 20*, 851–875, 1982.

Mellor, G. L., M G. McPhee, and M. Steele, Ice-seawater turbulent boundary layer interaction with melting or freezing, *J. Phys. Oceanogr., 16*, 1829–1846, 1986.

Røed, L. P., and J. J. O'Brien, A coupled ice-ocean model of upwelling in the marginal ice zone, *J. Geophys. Res., 88*, 2863–2872, 1983.

Thorndike, A. S., and R. Colony, Sea ice motion in response to geostrophic winds, *J. Geophys. Res., 87*, 5845–5852, 1982.

Turner, J. S., *Buoyancy Effects in Fluids*, 367 pp., Cambridge University Press, New York, 1973.

Zilitinkevich, S. S., Resistance laws and prediction equations for the depth of the planetary boundary layer, *J. Atmos. Sci., 32*, 741–752, 1975.

M. G. McPhee, McPhee Research Company, 371 Rolling Hills Drive, Yakima, WA 98908.

(Received March 20, 1986;
accepted September 16, 1986.)